Nanomanufacturing and Metrology (2022) 5:179–187
https://doi.org/10.1007/s41871-022-00140-y

ORIGINAL ARTICLE

Scanning and Splicing Atom Lithography for Self-traceable Nanograting Fabrication

Xiao Deng[1,2] · Wen Tan[1,2] · Zhaohui Tang[1,2] · Zichao Lin[1,2] · Xinbin Cheng[1,2] · Tongbao Li[1,2]

Received: 3 February 2022 / Revised: 21 March 2022 / Accepted: 24 March 2022 / Published online: 26 April 2022
© The Author(s) 2022

Abstract
Atom lithography is a unique method to fabricate self-traceable pitch standards and angle standards, but extending its structure area to millimeter-level for application is challenging. In this paper, on the one hand, we put forward a new approach to fabricate a full-covered self-traceable Cr nanograting by inserting and scanning a Dove prism in the Gaussian beam direction of atom lithography. On the other hand, we extend the structure area along the standing-wave direction by splicing two-step atom deposition. Both nanostructures manufactured via scanning atom lithography and splicing atom lithography demonstrate good pitch accuracy, parallelism, continuity, and homogeneity, which opens a new way to fabricate centimeter-level full-covered self-traceable nanograting and lays the basis for the application of square ruler and optical encoders at the nanoscale.

Keywords Scanning atom lithography · Splicing atom lithography · Nanograting · Self-traceability · Dove prism

1 Introduction

The utilization of fundamental natural constants plays a key role in the advancements in metrology for precise, reliable, reproducible, and accurate measurements with improved measurement uncertainties [1]. The recent revolutionary changes in SI unit redefinition in 2019 based on fundamental constants satisfy the increasing accuracy demands in science and industry, allowing the developments of quantum effect-based measurement techniques and providing in situ traceability to SI units for a wide range of users [2]. Self-traceability characteristics based on natural constants are also useful for accuracy improvements in nanometrology. For example, one-dimensional nanogratings, two-dimensional nanogratings, critical dimension (CD) structures, step height, and particles are the main kinds of length transfer standards at the nanoscale. Recently, the Si lattice constant has already been intensively used to fabricate self-traceable CD standards [3–6] and step height standards [7–9]. It has been proven to be an alternative approach to realize traceability in nanoscale dimension metrology [10–12].

Similarly, atom lithography has been demonstrated as a unique way to fabricate self-traceable pitch standards [13–15] and angle standards [16]. Atom lithography, or the so-called laser-focused atomic deposition, holds an accurate pitch, whose value is determined by the absolute transition frequency between two energy levels of an element, such as Cr [13], Fe [17], Al [18], Yb [19], and Ar [20]. Taking Cr atom lithography, for example, a series of one-dimensional nanogratings with different accurate pitches can be fabricated, such as 212.8 nm ($\lambda/2$) [15, 21], 106.4 nm ($\lambda/4$) [22], and 53.2 nm ($\lambda/8$) [21]. For the most investigated pitch of 212.8 nm, a previous diffraction measurement yielded a measurement mean pitch uncertainty to be 0.0069 nm, which agrees well with the theoretical mean pitch uncertainty limit of 0.0049 nm [15]. Recently, it has been approved as a first-class standard reference material (GBW13982) in China. Meanwhile, two-step Cr atom lithography is promising as a natural square ruler at the nanoscale [16]. It is expected to hold a natural orthogonal angle whose error is as small as 0.0027°. Moreover, a precision displacement measurement system based on a self-traceable grating interference has been proposed by the Littrow configuration, which shows direct traceable displacement measurement capabilities comparable to those of laser interferometers [23].

✉ Xinbin Cheng
chengxb@tongji.edu.cn

[1] MOE Key Laboratory of Advanced Micro-Structured Materials, Tongji University, Shanghai 200092, China

[2] Institute of Precision Optical Engineering, School of Physics Science and Engineering, Tongji University, Shanghai 200092, China

The structure area of atom lithography nanograting is challenging and necessary as a pitch standard for the applications. Generally, the structure area of atom lithography nanograting is determined by the shape parameter of the focusing laser field and atom flux source. To guarantee the power density for focusing, typically, the laser field radius at $1/e^2$ along the Gaussian direction is hard to extend to 250 μm [13, 24, 25]. To ensure the collimation of the atomic beam effusion, the width of the atomic beam deposition along the standing-wave direction is generally set to be 1 or 2 mm. The area size limits its application as a natural square ruler and optical encoder. Although an elliptical laser standing-wave field has been introduced to fabricate a millimeter-level nanostructure [26], the method coarsens the line edge of Cr nanograting, which increases the uncertainty of the pitch standard. Meanwhile, most of the atom fluxes along the Gaussian direction are not used during the deposition, which has wasted the collimated deposition materials to some degree.

Motivated by the aspects above, here, we propose a new approach to realize a millimeter-level self-traceable nanograting while keeping the standing-wave energy and atom flux full utilization at the same time. Analogous to e-beam lithography, we scanned the standing wave along the Gaussian direction to form a full-covered nanograting. Based on the scanning atom lithography, the structure width along the Gaussian direction was extended from 500 to 1500 μm. Based on splicing atom lithography, the structure width along the standing-wave direction was extended from 3 to 4.8 mm. Both methods have produced highly parallel, smooth, and unbroken self-traceable lines on the substrate. As expected, scanning and splicing atom lithography open a new way to fabricate self-traceable nanograting to millimeter-level and even centimeter-level areas. Hence, they lay the basis for highly homogeneous two-dimensional square ruler structures and self-traceable grating interferometers.

2 Theories and Experimental Design

2.1 Theories

In Cr atom lithography, the dipole force imposed on Cr atoms in the standing wave will focus the atom beam into lines to form self-traceable nanogratings. Their pitch is directly traceable to half of the laser light wavelength, which is strictly locked to a specified atomic level transition.

The energy level transition of chromium atom from the ground state $^7S_3$ to the excited state $^7P_4^0$ corresponds to the laser wavelength in the vacuum $\lambda = 425.55$ nm, with a natural linewidth $\Gamma = 5$ MHz. Although the excited state $^7P_4^0$ may also transits to the metastable states $^5D_3$ and $^5D_4$, it can be regarded as a two-level system because of its extremely small probability. The potential energy function of a two-level system can be written as [27, 28]

$$U(x,y,z) = \frac{\hbar\Delta}{2}\ln\left[1+\frac{I(x,y,z)}{I_s}\frac{\Gamma^2}{\Gamma^2+4\Delta^2}\right] \tag{1}$$

where $\hbar$ is the Planck's constant,Δ is the detuning of the laser frequency from the atomic resonance, $I(x,y,z)$ is the light intensity of the laser, and I_s is the saturation intensity of the atomic transition (for the chromium atom, $I_s = 85$ W/m^2). The light intensity formula of the standing-wave field formed by the Gaussian laser propagating along the x-axis and being reflected by the mirror can be expressed as [29]

$$I(x,y,z) = I_0\sin^2(kx)\exp\left(-\frac{2y^2}{\omega_y^2}-\frac{2z^2}{\omega_z^2}\right) \tag{2}$$

where x is the distance from the mirror surface; k is the number of waves of the laser; ω_y and ω_z are the beam waists of the laser in the y and z directions, respectively; and I_0 is the light intensity of the standing-wave field at anti-nodes.

As shown in Eqs. (1) and (2), for blue or red detuning, at the nodes of the standing-wave field ($I(x,y,z)=0$), the chromium atom has the lowest potential energy. Moreover, at the anti-nodes of the standing-wave field on the x-axis ($I(x,y,z)=I_0$), the chromium atom has the highest potential energy. Thus, for the blue detuning ($\Delta > 0$), chromium atoms converge at the nodes of the standing-wave field. Conversely, for the red detuning, the chromium atoms converge on the anti-nodes of the standing-wave field.

Particularly, in Eq. (2), if $x=0$, that is, on the surface of the mirror, $I(x,y,z)=0$. This value shows that the intensity at the mirror surface is always the node of the standing-wave field. If we keep the substrate and mirror relatively fixed in atomic lithography, then the positions of the standing-wave field nodes and anti-nodes on the substrate do not change. Hence, when we move the standing-wave field up and down parallelly, the trajectory of nodes and anti-nodes are parallel to the mirror.

2.2 Experimental Design for Scanning Atom Lithography

The working element of atom lithography is chromium obtained from our lab. The experimental system is shown in Fig. 1, and the laser configuration is demonstrated in Fig. 2. The entire experimental setup was placed on an optical platform. To obtain 425.55 nm of blue laser for the experiments, we used laser products from Coherent, Inc. to form a laser light source system with the following specifications: diode-pumped all-solid-state laser Verdi G-12, continuously adjustable single-frequency titanium gem laser MBR-110, and frequency multiplier MBD-200. Among



Fig. 1 Chromium atom lithography experimental system in Tongji University

them, Verdi G-12 can output a 532-nm continuous green laser with a maximum power of 11.5 W. MBR-110 can output an 851-nm near-infrared laser with a maximum power of 1.9 W under the pump of Verdi G-12, with a tunable range of 700–1000 nm. MBD-200 can output a 425.55-nm laser with a maximum power of 500 mW after doubling the laser output of MBR-110.

The chromium powder evaporated from an effusion cell, which was heated to 1625 ℃. The chromium atom flux passed the stabilization laser, cooling laser, and standing-wave in order. Collimated Cr atoms were focused to the node or anti-node of a standing wave grazing across the substrate surface.

As mentioned above, when we moved the standing-wave field up and down parallelly, the trajectory of nodes and anti-nodes were parallel to the mirror. Therefore, we propose a method called scanning atom lithography, which is illustrated in Fig. 3. The main difference of scanning atom

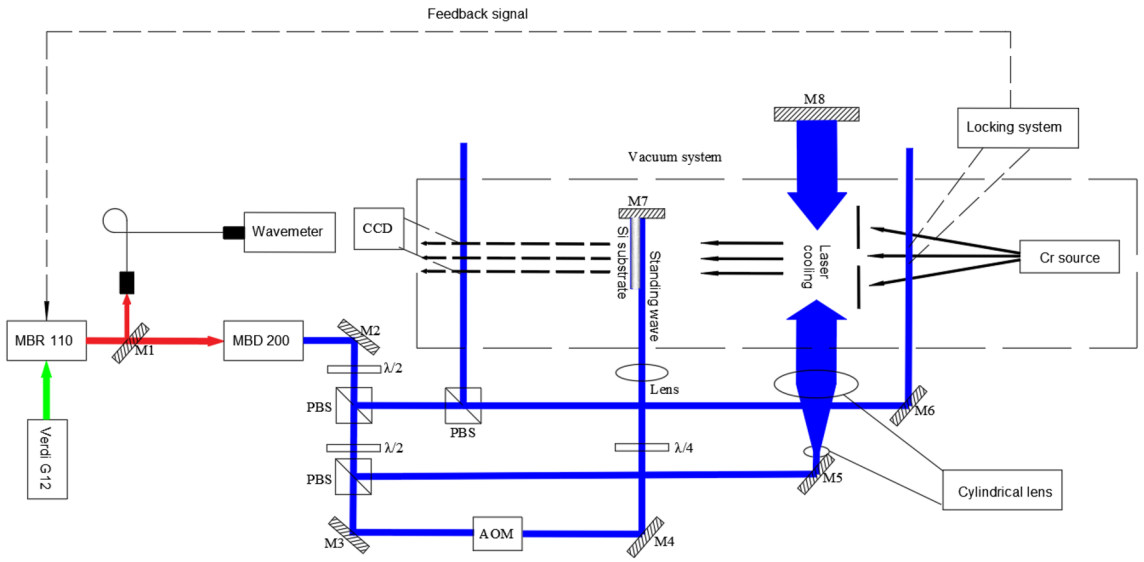


Fig. 2 Laser configuration of Cr atom lithography

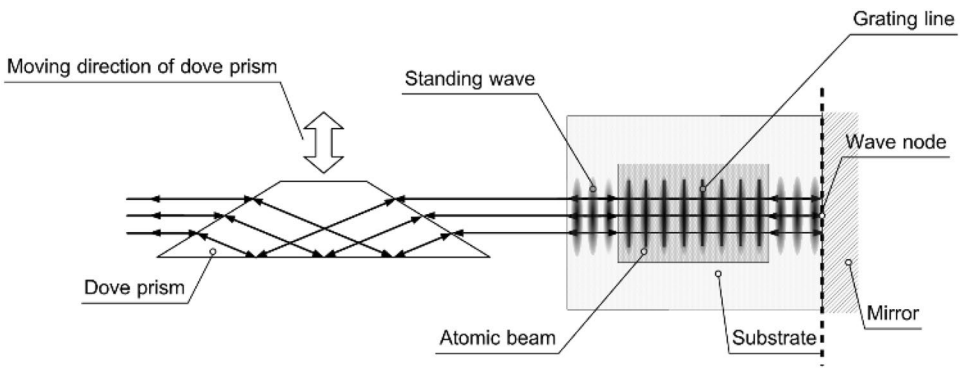


Fig. 3 Schematic design of scanning atom lithography

lithography to the normal setup is that we insert a Dove prism for the standing-wave adjustment. The Dove prism was produced by Union Optic, Wuhan, China. The product model is DVP0110, the vertical direction of the movable height is 10 ± 0.2 mm, the bottom angle is 45°, the angle error is less than 3′, and the surface roughness is 0.6–1.5 nm. Generally, the Dove prism is designed to invert an image. Here it was used for changing the height of the standing-wave parallelly and "scanning" the whole Cr atom beam flux after a slit.

In the experiment, the slowly moving Dove prism scanned the whole Cr atom flux to form a full-covered nanograting. Figure 4 shows the standing-wave configuration at different locations along the Gaussian direction. Because the standing-wave status at the mirror is nodes all the time, it will not change the parallelism of nanograting. Moreover, the prism motion will hardly change the optical path of the standing wave, and only the mirror surface waviness will influence the position of every grating profile. Because the surface roughness of the mirror coating can be controlled at the sub-nanometer level, the distance between the mirror and laser beam radius waist will not change during scanning. By keeping the stability of the mirror-laser beam waist superposition, the self-traceable nanograting holds a good uniformity at trans-scale.

2.3 Experimental Design for Splicing Atom Lithography

Splicing atom lithography relates to a method for extending the structure area along the standing-wave direction. It comprises the steps illustrated in Fig. 5. The direction of the incident laser will stay unchanged during both processes. However, in this study, we moved the main lens, substrate, and mirror along the standing-wave direction for a certain distance and fixed the reflection to complete the exact coincidence with the incident laser. The two atom lithography processes will form an overlapping area to make the atom lithography grating lines "spliced" at the overlapping area, thus extending the length of the line area along the standing wave. Repeated splicing operations can be subsequently performed as needed, and each operation process is consistent with the above splicing operations.

For splicing atomic lithography, it is extremely important to control the grating line error in the overlapping area, including the grating line parallelism and grating pitch consistency. Fortunately, the basic principles of atomic lithography determine that this splicing atomic lithography is perfect splicing in theory. During the whole process of splicing atomic lithography, we moved the substrate, standing-wave beam radius, and reflection mirror as a whole, and the phase of the mirror position was always at the node status of the standing-wave field. Therefore, for every deposition, the phase of the standing-wave field formed at a specific position away from the mirror was exactly the same and fixed all

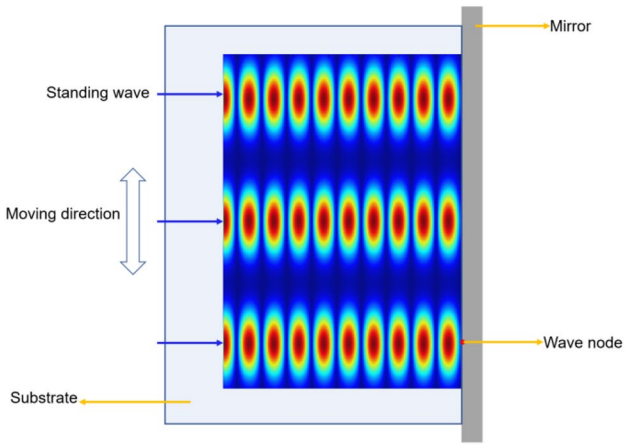


Fig. 4 Standing-wave configuration at different locations along the Gaussian direction

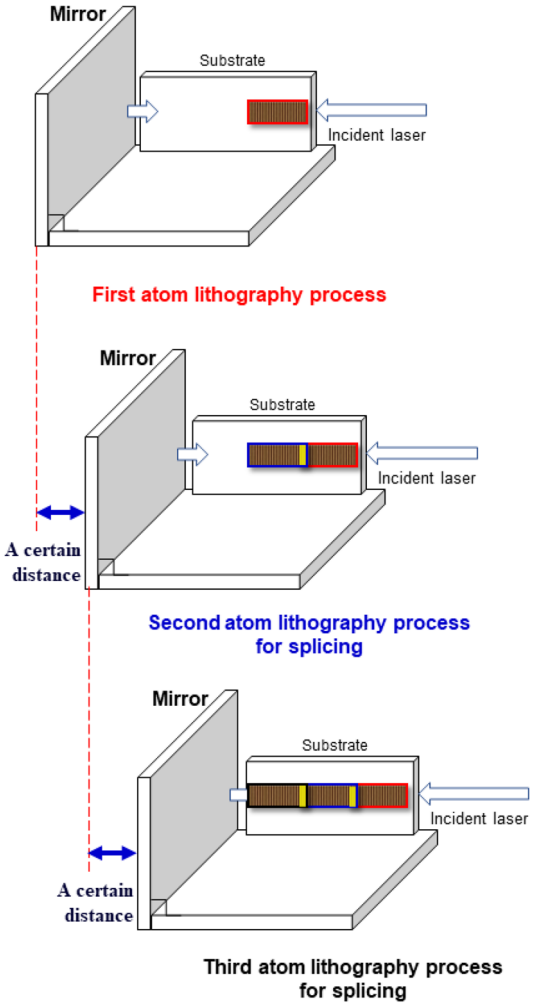


Fig. 5 Schematic design of splicing atom lithography

the time if there is no relative movement between the reflection mirror and substrate. This condition lays the theoretical foundation for perfect splicing. In the overlapping area, the result of perfect splicing is that the height of the grating will increase, but this has no effect on the calculation of the parameter of the mean pitch. Therefore, splicing atomic lithography is based on perfect splicing. The length of the grating along the standing-wave direction was extended, which provides a perfect solution for solving the problem of range expansion in the use of the grating as an encoder.

3 Experimental Results and Discussion

3.1 Scanning Atom Lithography Along the Gaussian Direction

Next, we conducted the scanning atom lithography experiment as designed. The slit size was 3 mm along the standing-wave direction and 1.5 mm along the Gaussian beam direction. We fixed the Dove prism to a vertical stage with the KSMV6-40ZF model. It was built with a total travel range of 6 mm and a sensitivity of 2 μm. During the scanning process, we moved the standing-wave vertically by 100 μm every 20 min. The total scanning time was 5 h. For the laser beam part, the power of the stabilization laser beam, cooling laser beam, and focusing laser beam are 8, 25, and 60 mW, respectively. The cutting proportion of the focusing laser beam was approximately 45% during the whole process.

Figure 6 shows the monitor record of the laser frequency before frequency doubling during the process. In Fig. 6, the laser wavelength stabilized at 851.10691 nm throughout the deposition process. Although the wavelength of the laser frequency rapidly fluctuated, it was quickly locked at the position of the atomic transition frequency by the frequency locking system. During the whole process, the laser wavelength error that affects the atomic lithography grating should not exceed 4×10^{-6} nm. Since the nanograting pitch is only a quarter of this wavelength, the pitch difference at the deposition area varied by approximately 1×10^{-6} nm. The extremely high stabilization of the frequency lays the basis for a highly uniform nanograting fabrication.

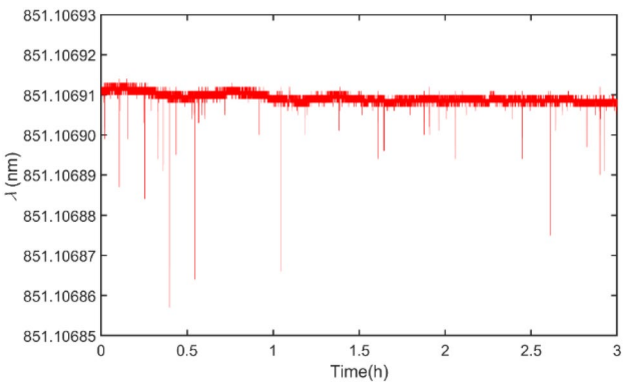


Fig. 6 Laser wavelength oscillation during scanning atom lithography

The parallelism and continuity of the nanograting are also the main characteristics of scanning atom lithography. We randomly selected a "mapping" measurement reference line along the Gaussian direction for the scanning electron microscope measurement. Figure 7a shows a typical image of Cr nanograting, where all the lines are highly parallel and have no adhesions. Figure 7b shows the peak-to-valley-height (PTVH) distribution along the Gaussian direction. After a careful examination of all the images, no misplacement and bridging phenomenon exists.

Scanning atom lithography lowers the production efficiency to some degree. However, in fact, if we take the structure size and vacuum system pumping time into account, it increases the production efficiency. In subsequent studies,

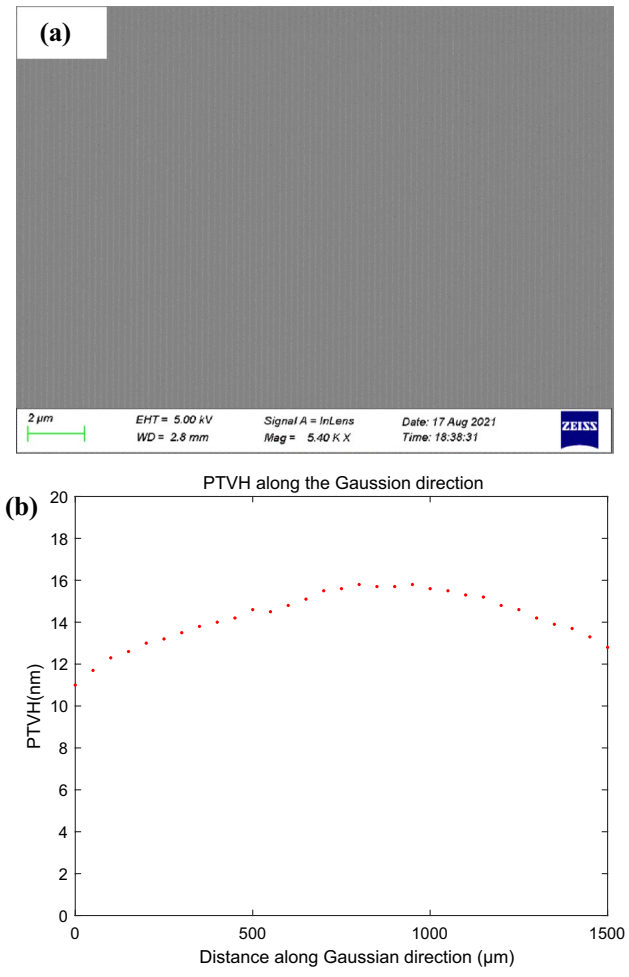


Fig. 7 **a** SEM image of Cr nanograting along the Gaussian direction; **b** peak-to-valley-height distribution along the Gaussian direction

we will continue to optimize the fabrication process, such as increasing the deposition rates and laser power density.

3.2 Splicing Atom Lithography Along the Standing-Wave Direction

Similarly, we arranged the splicing atom lithography process based on the previous experimental design, and two atom lithography depositions were performed. Figure 8 is an optical image of the grating region formed by splicing atom lithography and AFM images from P_1 to P_7 of the grating area along the standing-wave direction. First, in the optical image, there is an overlapping deposition area between the two atom lithography processes. The deposition color in the overlapping area is significantly brighter than that in the area deposited alone, mainly due to the increase in the thickness of the atomic deposition film. Second, in the AFM image, the grating lines of the first deposition area, second deposition area, and overlapping deposition area are all of good quality, and the pitches are all the same. This finding preliminarily shows that perfect stitching occurs in the process of splicing atom lithography.

Other evidence for the perfect stitching is the height of the deposited gratings in different regions. In the optical image in Fig. 8, we made a graph of the PTVH of the grating changing with the position along the standing-wave direction in 50-μm steps, as shown in Fig. 9.

Typical values for the first and second atomic lithography grating PTVHs are basically 15–22 nm, respectively. A typical value of the PTVHs of the overlapping area grating is 23–32 nm. This value range can illustrate two key issues: On the one hand, the grating height of the overlapping part is very close to the sum of the first and second grating heights. Hence, the second deposition process grows on the basis of the first deposition grating, and the peaks and troughs correspond one-to-one. On the other hand, the height of the grating in the overlapping part is smaller than the sum of the heights of the first and second deposition area gratings, and the half-height width is slightly larger than the two. As a result, the grating will be widened due to the shading effect in addition to the process of the height increase, which is consistent with our previous observations. Based on these two aspects of analysis, the proposed splicing atom lithography technology achieves the perfect expansion of the grating area in the direction of the standing-wave field with confidence.

3.3 Pitch Error Analysis

In previous studies, Jabez McClelland's group performed an error analysis of the atom lithography deposition [15]. By contrast, our splicing and scanning atom lithography involve multiple atom lithography depositions; the standing-wave field moves along the mirror in scanning atom lithography, and the position change in splicing atom lithography results in an additional pitch error. Therefore, it is necessary to perform error analysis. Here, we mainly analyzed three error sources brought about by scanning and splicing atom lithography: the non-parallelism of the mirror surface,

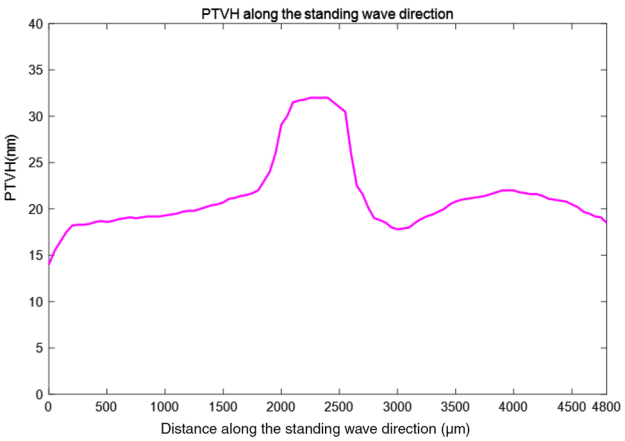


Fig. 9 Peak-to-valley height of Cr grating along the standing-wave direction for splicing atom lithography

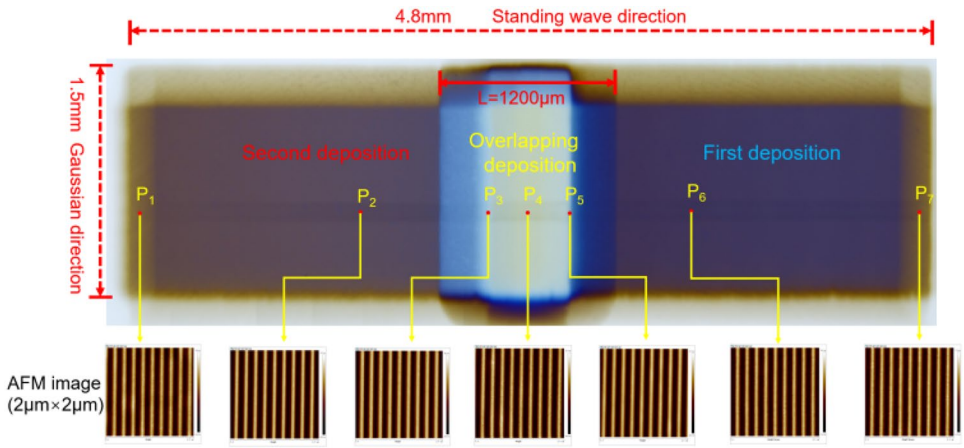


Fig. 8 Optical image of deposition areas and AFM image of grating lines in splicing atom lithography

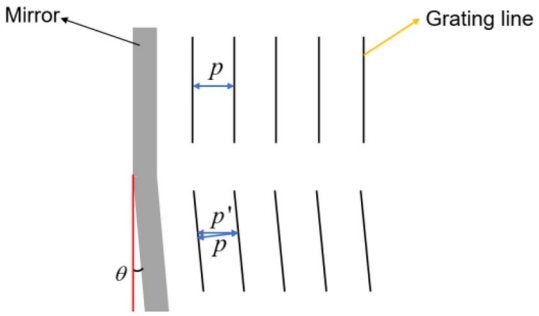


Fig. 10 Effect of the mirror non-parallelism on scanning atom lithography

the non-coincidence of the standing wave, and the Gaussian beam phase shift.

3.3.1 Error Caused by the Non-parallelism of the Mirror Surface

In scanning atom lithography, there are continuous movements of the standing wave along the mirror surface. Because the mirror surface is not absolutely flat, there is a pitch error of mirror non-parallelism. The error caused by the non-parallelism of the mirror surface is shown in Fig. 10.

The error caused by the mirror non-parallelism is given by Eq. (3):

$$\Delta p = p' - p = \frac{p}{\cos\theta} - p \tag{3}$$

where θ is the angle caused by the uneven mirror surface and p is the pitch of grating. The mirror surface non-parallelism we used is $< 5'$, resulting in a pitch error of 2.2×10^{-4} nm.

3.3.2 Error caused by the Non-coincidence of the Standing-Wave

Similar to the mirror's non-parallelism, the Dove prism also has a geometric defect, which will change the angle of incidence of the incident Gaussian laser and cause the reflected light to not coincide with the incident light. A diaphragm was installed 1 m from the mirror to observe the coincidence of the incident light and reflected light. In the process of scanning atom lithography, the movement of the Dove prism hardly changed the non-coincidence of the reflected light with the incident light. We estimated the pitch error based on [15], and the pitch error caused by the non-coincidence of incident light and reflected light was as small as 2.5×10^{-5} nm.

Table 1 Additional error in scanning and splicing atom lithography

Source	Pitch error (nm)
Non-parallelism of the mirror surface	2.2×10^{-4}
Non-coincidence of the standing-wave	2.5×10^{-5}
Gaussian beam phase shift	
Caused by the Dove prism	1.6×10^{-5}
Caused by splicing atom lithography	3.9×10^{-4}
Total	4.5×10^{-4}

3.3.3 Error Caused by the Gaussian Beam Phase Shift

Because Gaussian beams acquire phase shifts in the direction of propagation, this phase shift differs from the phase shift of plane waves propagating at the same optical frequency. This difference is known as the Gaussian beam phase shift. The phase shift produced by the Gaussian beam is given by Eq. (4) [30]:

$$\phi_G = -\arctan(z/z_R) \tag{4}$$

where z is the axial distance from the beam waist, $z_R = \pi\omega_0^2/\lambda$ is the Rayleigh range of the Gaussian beam, λ is the wavelength, and ω_0 is the $1/e^2$ beam radius at the waist. The pitch error produced by the phase shift of the Gaussian beam in single-time atom lithography is [15]

$$\Delta z = \frac{\lambda}{2\pi}\left[\arctan(z_2/z_R) - \arctan(z_1/z_R)\right] \tag{5}$$

For our splicing atom lithography experiment this time, $z_2 = 6.8$ mm, $z_1 = 2$ mm; beam waist ω_0 was 70 μm, which was measured using a laser beam profiler (LBP2-HR-VIS2, Newport, California, USA). Thus, $z_R = 36.2$ mm. The total error resulting from the Gaussian beam phase shift was $\Delta z = 8.84$ nm, and the pitch error for 4.8 mm was 3.9×10^{-4} nm. In addition, due to the geometric defects in the Dove prism, such as surface roughness (0.6–1.5 nm) and angular error (less than 3′), additional optical path differences were created during the movements. The optical path difference of 1.5 mm brought by the vertically moving Dove prism was less than 0.2 mm, so the pitch error caused by the Dove prism for 4.8 mm was less than 1.6×10^{-5} nm.

We enumerate the additional errors generated by scanning atom lithography and splicing atom lithography in Table 1. As can be seen in the table, splicing atom lithography and scanning atom lithography introduced a mean pitch error of 4.5×10^{-4} nm. Because this error is too small compared to the previously calculated 0.0049 nm [15], the theoretical pitch of our system's atom lithography grating remained at 212.7787 ± 0.0049 nm. Hence, both nanostructures manufactured via scanning atom lithography and splicing atom lithography will demonstrate good pitch accuracy, parallelism, continuity, and homogeneity.

4 Conclusions

To summarize, in this paper, we put forward the scanning atom lithography method and splicing atom lithography method to extend the structure area of self-traceable nanogratings along the Gaussian direction and standing-wave direction, respectively. By inserting and scanning a Dove prism in the standing-wave direction, the Cr nanograting area extended from 500 to 1500 μm. By splicing two atom lithography areas together, we achieved a perfect expansion of the grating area from 3 to 4.8 mm in the direction of the standing-wave field with confidence. Based on the experimental results and pitch error analysis, both nanostructures manufactured via scanning atom lithography and splicing atom lithography demonstrated good pitch accuracy, parallelism, continuity, and homogeneity. Therefore, scanning atom lithography and splicing atom lithography open a new way to fabricate centimeter-level full-covered self-traceable nanograting, which lay the basis for the useful applications of square rulers and optical encoders at the nanoscale.

Acknowledgements This work was supported by Significant Development Project of Shanghai Zhangjiang National Innovation Benchmarking Zone (Grant No. ZJ2021-ZD-008); National Natural Science Foundation of China (Grant No.62075165); Science and Technology Commission of Shanghai (Grant No. 208014043); Shanghai Municipal Science and Technology Major Project (2021SHZDZX0100) and the Fundamental Research Funds for the Central Universities; Opening Fund from Shanghai Key Laboratory of Online Detection and Control Technology of SIMT.

Declarations

Conflict of interest The authors declare that we have no competing interest for this paper.

Open Access This article is licensed under a Creative Commons Attribution 4.0 International License, which permits use, sharing, adaptation, distribution and reproduction in any medium or format, as long as you give appropriate credit to the original author(s) and the source, provide a link to the Creative Commons licence, and indicate if changes were made. The images or other third party material in this article are included in the article's Creative Commons licence, unless indicated otherwise in a credit line to the material. If material is not included in the article's Creative Commons licence and your intended use is not permitted by statutory regulation or exceeds the permitted use, you will need to obtain permission directly from the copyright holder. To view a copy of this licence, visit http://creativecommons.org/licenses/by/4.0/.

References

1. Yadav S, Aswal DK (2020) Redefined SI units and their implications. MAPAN 35:1–9
2. Stock M, Davis R, de Mirandés E, Milton MJT (2019) The revision of the SI—the result of three decades of progress in metrology. Metrologia 56:022001
3. Dixson RG, Allen RA, Guthrie WF, Cresswell MW (2005) Traceable calibration of critical-dimension atomic force microscope linewidth measurements with nanometer uncertainty. J Vac Sci Technol B Microelectron Nanometer Struct 23:3028
4. Dai G, Heidelmann M, Kübel C, Prang R, Fluegge J, Bosse H (2013) Reference nano-dimensional metrology by scanning transmission electron microscopy. Meas Sci Technol 24:085001
5. Dai G, Zhu F, Heidelmann M, Fritz G, Bayer T, Kalt S, Fluegge J (2015) Development and characterisation of a new line width reference material. Meas Sci Technol 26:115006
6. Dai G, Hahm K, Bosse H, Dixson RG (2017) Comparison of line width calibration using critical dimension atomic force microscopes between PTB and NIST. Meas Sci Technol 28:065010
7. Orji NG, Dixson RG, Fu J, Vorburger TV (2004) Traceable pico-meter level step height metrology. Wear 257:1264–1269
8. Sheglov DV, Kosolobov SS, Fedina LI, Rodyakina EE, Gutakovskii AK, Sitnikov SV, Kozhukhov AS, Zagarskikh SA, Kopytov VV, Evgrafov VI, Shuvalov GV, Matveichuk VF, Latyshev AV (2013) High-precision nanoscale length measurement. Nanotechnol Russia 8:518–531
9. He BC, Fu WE, Wu CL, Chien YS, Liou HC (2015) Calibrating the Z-magnification of atomic force microscope below 10 nm by single-atom steps. Thin Solid Films 584:372–377
10. Dai G, Koenders L, Fluegge J, Bosse H (2016) Two approaches for realizing traceability in nanoscale dimensional metrology. Opt Eng 55:091407
11. Garnæs J, Nečas D, Nielsen L, Madsen MH, Torras-Rosell A, Zeng G, Klapetek P, Yacoot A (2020) Algorithms for using silicon steps for scanning probe microscope evaluation. Metrologia 57:064002
12. Yacoot A, Bosse H, Dixson R (2020) The lattice parameter of silicon: a secondary realisation of the metre. Meas Sci Technol 31:121001
13. McClelland JJ, Scholten RE, Palm EC, Celotta RJ (1993) Laser-focused atomic deposition. Science 262:877–880
14. Gupta R, McClelland JJ, Jabbour ZJ, Celotta RJ (1995) Nanofabrication of a two-dimensional array using laser-focused atomic deposition. Appl Phys Lett 67:1378–1380
15. McClelland JJ, Anderson WR, Bradley CC, Walkiewicz M, Celotta RJ, Jurdik E, Deslattes RD (2003) Accuracy of nanoscale pitch standards fabricated by laser-focused atomic deposition. J Res Natl Inst Stand Technol 108:99–113
16. Deng X, Liu J, Zhu L, He P, Cheng X, Li T (2018) Natural square ruler at nanoscale. Appl Phys Express 11:075201
17. te Sligte E, Smeets B, van der Stam KMR, Herfst RW, van der Straten P, Beijerinck HCW, van Leeuwen KAH (2004) Atom lithography of Fe. Appl Phys Lett 85:4493–4495
18. McGowan RW, Giltner DM, Lee SA (1995) Light force cooling, focusing, and nanometer-scale deposition of aluminum atoms. Opt Lett 20:2535
19. Ohmukai R, Urabe S, Watanabe M (2003) Atom lithography with ytterbium beam. Appl Phys B 77:415–419
20. Johnson KS, Thywissen JH, Dekker NH, Berggren KK, Chu AP, Younkin R, Prentiss M (1998) Localization of metastable atom beams with optical standing waves: nanolithography at the Heisenberg limit. Science 280:1583–1586
21. McClelland JJ, Celotta RJ (2000) Laser-focused atomic deposition—nanofabrication via atom optics. Thin Solid Films 367:25–27
22. Schulze T, Brezger B, Schmidt PO, Mertens R, Bell AS, Pfau T, Mlynek J (1999) Sub-100 nm structures by neutral atom lithography. Microelectron Eng 46:105–108

23. Xiao D, Xinbin C, Zichao L, Zhenjie G, Yulin Y, Tongbao L (2021) System for precision displacement measurement based on self-traceable grating interference. Chin Patent 32:175301
24. Drodofsky U, Stuhler J, Brezger B, Schulze T, Drewsen M, Pfau T, Mlynek J (1997) Nanometerscale lithography with chromium atoms using light forces. Microelectron Eng 35:285–288
25. Deng X, Li TB, Lei LH, Ma Y, Ma R, Weng JJ, Li Y (2014) Fabrication and measurement of traceable pitch standard with a big area at trans-scale. Chin Phys B 23:090601
26. Zhang T, Yin C, Zhao Y, Qian J, Wang J, Shi C (2018) Nanofabrication of millimeter-level nanostructure via laser-focused atomic deposition. Appl Phys Express 11:092003
27. Dalibard J, Cohentannoudji C (1985) Dressed-atom approach to atomic motion in laser-light—the dipole force revisited. J Opt Soc Am B 2:1707–1720
28. Mcclelland JJ (1995) Atom-optical properties of a standing-wave light-field. J Opt Soc Am B 12:1761–1768
29. Petra SJH, van Leeuwen KAH, Feenstra L, Hogervorst W, Vassen W (2003) Numerical simulations on the motion of atoms travelling through a standing-wave light field. Eur Phys J D 27:83–91
30. Feng S, Winful HG (2001) Physical origin of the Gouy phase shift. Opt Lett 26:485–487